Hybrid First-Principles/Neural Networks Model for Column Flotation

Sanjay Gupta, Pi-Hsin Liu, and Spyros A. Svoronos
Dept. of Chemical Engineering, University of Florida, Gainesville, FL 32611

Rajesh Sharma, N. A. Abdel-Khalek, Yahui Cheng, and Hassan El-Shall
Dept. of Materials Science and Engineering, University of Florida, Gainesville, FL 32611

A new model for phosphate column flotation is presented which for the first time relates the effects of operating variables such as frother concentration on column performance. This is a hybrid model that combines a first-principles model with artificial neural networks. The first-principles model is obtained from material balances on both phosphate particles and gangue (undesired material containing mostly silica). First-order rates of net attachment are assumed for both. Artificial neural networks relate the attachment rate constants to the operating variables. Experiments were conducted in a 6-in.-dia. (152-mm-dia.) laboratory column to provide data for neural network training and model validation. The model successfully predicts the effects of frother concentration, particle size, air flow rate and bubble diameter on grade and recovery.

Introduction

Flotation is a process in which air bubbles are used to separate a hydrophobic from a hydrophilic species. The majority of the hydrophobic materials get attached to the bubbles and leave with the froth from the top of a cell or column separator, while the hydrophilic material leaves from the bottom. This process is commonly used in the minerals industry, including the phosphate industry, in which the phosphate containing rock (frankolite or apatite) is to be separated from gangue (mostly silica). Flotation is also used to remove oil from wastewater and to remove ink from paper pulp. In anionic phosphate flotation, the mineral is first treated with fatty acid collector and fuel oil extender. At proper concentrations they mostly adsorb on the phosphate-containing particles rendering them hydrophobic. Then, the phosphate-containing particles are separated from gangue via the flotation process. The majority of the phosphate plants employ mechanical cells. However, column flotation has simpler operation and provides superior grade/recovery performance. For these reasons, column flotation is gaining increasing acceptance for the processing and beneficiation of phosphate ores.

Column flotation is frequently employed for the recovery of other minerals (such as coal, copper, nickel, and gold). In such applications, the column can be divided into three zones: an upper froth zone, a lower collection zone, and an intermediate interface zone. An additional "wash water" stream is usually added from the top of the column. Phosphate flotation deals with considerably larger particles of size 0.1-1 mm. As a result, instead of wash water from the top, elutriation water from the bottom is added. Furthermore, columns are typically operated with negligible froth and interface zones. This considerably simplifies the modeling effort, as only the collection zone needs to be accounted for.

Particle transport in the collection zone is usually modeled as axial convection coupled with axial dispersion. The Peclet number (Pe), or its inverse, the dispersion number, governs the degree of mixing. Most models only consider the slurry phase (Finch and Dobby, 1990; Luttrell and Yoon, 1993), in which case particle collection is viewed as a first-order net attachment rate process. A model that considers both slurry and air phase was developed by Sastry and Loftus (1988). In

Correspondence concerning this article should be addressed to S. A. Svoronos.

this case, particle attachment and detachment are modeled separately with first-order rates. Luttrell and Yoon (1993) used a probabilistic approach to relate the particle net attachment rate constant to some operating variables (e.g., air flow rate). Their approach, however, involves empirical parameters, and it cannot be used to predict the effect of certain operating variables such as the frother and collector concentrations.

In this work, we use neural networks to determine the dependence of the phosphate and gangue flotation rate constants on the operating variables. Artificial neural networks have the ability to approximate any smooth nonlinear multivariable function arbitrarily well (Hornik et al., 1989). This approach can be used to determine the dependence of the performance of a flotation column (i.e., grade and recovery) on any operational variable. We demonstrate it in this work by developing a hybrid model that predicts the effect of frother concentration, air flow rate, feed rate and loading, elutriation flow rate, tailings flow rate, and particle size distribution.

The idea of developing a hybrid model by combining a first-principles model (FPM) with artificial neural networks (ANNs) is not new. Johansen and Foss (1992) and Su et al. (1992) proposed parallel structures where the output of the hybrid model is a weighted sum of the first-principles and ANN models. Kramer et al. (1992) proposed a parallel arrangement of a default model (which could be a first principles model) and a radial basis function ANN. An alternative approach is to combine ANNs with a FPM in a serial fashion, by using the ANNs to develop expressions for the FPM parameters or rate expressions. Psichogios and Ungar (1992a,b) proposed this scheme for parameters that are functions of the state variables and manipulated inputs, and trained the neural networks (i.e., determined the neural network parameters) on the error of the output of the first-principles model. A similar approach was followed by Reuter et al. (1993) to model metallurgy and mineral processes. Liu et al. (1995) developed a hybrid model for a periodic wastewater treatment process by using ANNs for the biokinetic rates of a first-principles model. The Psichogios and Ungar (1992a,b) approach was used by Cubillo et al. (1996) to model particulate drying processes and by Cubillo and Lima (1997) to develop a hybrid model for a rougher flotation circuit. Thompson and Kramer (1994) combined the parallel and serial hybrid modeling approaches.

As in the Psichogios and Ungar (1992a,b) approach, the hybrid model presented here uses backpropagation ANNs for certain parameters of a FPM. Instead of training these ANNs on the errors of the measured outputs of the FPM (grade and recovery), however, it inverts the FPM for each set of measurements to calculate corresponding parameter values and trains the ANNs on the errors of the calculated parameter values. Another innovation of this hybrid model is that it involves two levels of neural networks. This structure has the advantage that if certain factors affecting the process like the type of frother or air sparger used are changed, only the top-level neutral networks need to be retrained. These only require experimental data that can be easily obtained with short experiments that do not involve rock, and the large database of past grades and recoveries is still valid and does not need to be replaced. Finally, in contrast to the above referenced works, the hybrid model presented here is developed with experimental data instead of simulated data.

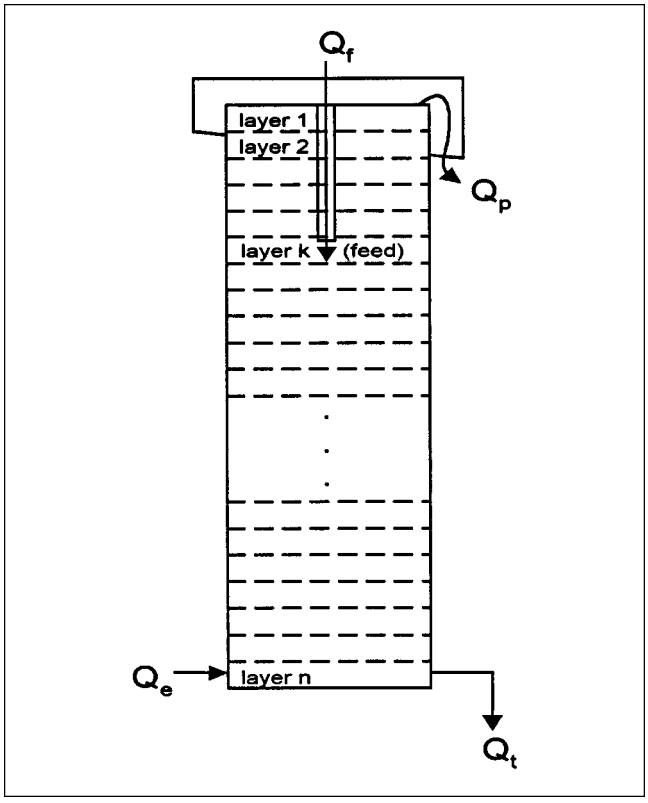

Figure 1. Column for phosphate flotation.

First-Principles Model

The FPM is obtained from material balances on both phosphate and gangue. It neglects radial dispersion and changes in the air holdup. Following Luttrell and Yoon (1993), the particle to bubble attachment and detachment rates are combined in one net attachment rate, and this rate is assumed to be first order with respect to particle concentration in the slurry.

The model subdivides the column into n layers as shown in Figure 1. Feed containing both the desired (phosphate) and undesired (gangue) particles enters in a slurry in layer k. An additional inlet stream is the elutriation water that enters in the bottom of the column (layer n). Most of that flow is due to water that enters with the air sparger, as most of the popular spargers are two-phase and introduce a considerable amount of water. There are two outlet streams: the tailings stream through the bottom of the column (layer n) that contains mostly gangue, and the product (concentrate) stream that leaves from the top of the column.

The particles are subdivided into size ranges according to the standard Tyler mesh screens. Particles of a certain mesh are considered to have diameter the geometric mean of the lower and upper limits. As the attachment rate constants and particle slip velocities depend on particle size, a separate material balance is written for each mesh size. The air holdup is assumed constant. Material balances at each layer yield the following equations for the phosphate particles:

Layer 1 (top)

$$\frac{dC_{p_1}^j}{dt}=\begin{cases}\left(\dfrac{U_p}{1-\epsilon_g}-U_{sl}^j\right)\dfrac{C_{p_2}^j-C_{p_1}^j}{\Delta z}+D\dfrac{C_{p_2}^j-C_{p_1}^j}{\Delta z^2}-k_p\left(d_p^j\right)C_{p_1}^j & \text{if} \quad U_{sl}^j\le\dfrac{U_p}{1-\epsilon_g}\\ -\left(U_{sl}^j-\dfrac{U_p}{1-\epsilon_g}\right)\dfrac{C_{p_1}^j}{\Delta z}+D\dfrac{C_{p_2}^j-C_{p_1}^j}{\Delta z^2}-k_p\left(d_p^j\right)C_{p_1}^j & \text{if} \quad U_{sl}^j>\dfrac{U_p}{1-\epsilon_g}\end{cases} \tag{1}$$

Layer 2 to $k-1$; $k=$ feed layer

$$\frac{dC_{p_i}^j}{dt}=\begin{cases}\left(\dfrac{U_p}{1-\epsilon_g}-U_{sl}^j\right)\dfrac{C_{p_{i+1}}^j-C_{p_i}^j}{\Delta z}+D\dfrac{C_{p_{i+1}}^j-2C_{p_i}^j+C_{p_{i-1}}^j}{\Delta z^2}-k_p\left(d_p^j\right)C_{p_i}^j & \text{if} \quad U_{sl}^j\le\dfrac{U_p}{1-\epsilon_g}\\ \left(U_{sl}^j-\dfrac{U_p}{1-\epsilon_g}\right)\dfrac{C_{p_{i-1}}^j-C_{p_i}^j}{\Delta z}+D\dfrac{C_{p_{i+1}}^j-2C_{p_i}^j+C_{p_{i-1}}^j}{\Delta z^2}-k_p\left(d_p^j\right)C_{p_i}^j & \text{if} \quad U_{sl}^j>\dfrac{U_p}{1-\epsilon_g}\end{cases} \tag{2}$$

Feed Layer = k

$$\frac{dC_{p_k}^j}{dt}=\begin{cases}\dfrac{\left(Q_f/A_c\right)C_f^j-\left(\dfrac{U_p}{1-\epsilon_g}-U_{sl}^j\right)C_{p_k}^j-\left(\dfrac{U_t}{1-\epsilon_g}+U_{sl}^j\right)C_{p_k}^j}{\Delta z}+D\dfrac{C_{p_{k+1}}^j-2C_{p_k}^j+C_{p_{k-1}}^j}{\Delta z^2}-k_p\left(d_p^j\right)C_{p_k}^j & \\ & \text{if} \quad U_{sl}^j\le\dfrac{U_p}{1-\epsilon_g}\\ \dfrac{\left(Q_f/A_c\right)C_f^j+\left(U_{sl}^j-\dfrac{U_p}{1-\epsilon_g}\right)C_{p_{k-1}}^j-\left(\dfrac{U_t}{1-\epsilon_g}+U_{sl}^j\right)C_{p_k}^j}{\Delta z}+D\dfrac{C_{p_{k+1}}^j-2C_{p_k}^j+C_{p_{k-1}}^j}{\Delta z^2}-k_p\left(d_p^j\right)C_{p_k}^j & \\ & \text{if} \quad U_{sl}^j>\dfrac{U_p}{1-\epsilon_g}\end{cases} \tag{3}$$

Layer $k+1$ to $n-1$

$$\frac{dC_{p_i}^j}{dt}=\left(\frac{U_t}{1-\epsilon_g}+U_{sl}^j\right)\frac{C_{p_{i-1}}^j-C_{p_i}^j}{\Delta z}+D\frac{C_{p_{i+1}}^j-2C_{p_i}^j+C_{p_{i-1}}^j}{\Delta z^2}-k_p\left(d_p^j\right)C_{p_i}^j \tag{4}$$

Layer n (bottom)

$$\frac{dC_{p_n}^j}{dt}=\begin{cases}\dfrac{\left(\dfrac{U_t}{1-\epsilon_g}+U_{sl}^j\right)C_{p_{n-1}}^j-\left(\dfrac{Q_t}{\left(1-\epsilon_g\right)A_c}+U_{sl}^j\right)C_{p_n}^j}{\Delta z}+D\dfrac{C_{p_{n-1}}^j-C_{p_n}^j}{\Delta z^2}-k_p\left(d_p^j\right)C_{p_n}^j & \text{if} \quad U_{sl}^j\ge-\dfrac{U_t}{1-\epsilon_g}\\ \dfrac{\left(\dfrac{U_t}{1-\epsilon_g}+U_{sl}^j\right)C_{p_n}^j-\left(\dfrac{Q_t}{\left(1-\epsilon_g\right)A_c}+U_{sl}^j\right)C_{p_n}^j}{\Delta z}+D\dfrac{C_{p_{n-1}}^j-C_{p_n}^j}{\Delta z^2}-k_p\left(d_p^j\right)C_{p_n}^j & \text{if} \quad U_{sl}^j<-\dfrac{U_t}{1-\epsilon_g}\end{cases} \tag{5}$$

where

A_c = cross-sectional area of the column
C_f^j = phosphate feed concentration of jth mesh size particles
$C_{p_i}^j$ = phosphate concentration of jth mesh size particles in the ith layer
Q_f = feed volumetric flow rate
Q_t = tailings volumetric flow rate
Q_e = elutriation volumetric flow rate
Q_p = product volumetric flow rate

U_p = superficial liquid velocity above the feed point $= Q_p/A_c$
U_t = superficial liquid velocity below the feed point $= (Q_t - Q_e)/A_c$
U_{sl}^j = slip velocity of jth mesh size particles
ϵ_g = air holdup
$k_p(d_p^j)$ = flotation rate constant for phosphate for jth mesh size particles

The slip velocity is calculated using the expression of Villeneueve et al. (1996):

$$U_{sl}^j = \frac{g d_p^{j^2}(\rho_s - \rho_l)(1-\phi_s)^{2.7}}{18\mu_l\left(1+0.15R_{ep}^{j^{0.687}}\right)} \tag{6}$$

where the particle Reynolds number is defined as

$$R_{ep}^j = \frac{d_p^j U_{sl}^j \rho_s(1-\phi_s)}{\mu_l} \tag{7}$$

where
g = acceleration due to gravity (m/s^2)
μ_l = water viscosity (kg/m·s)
ρ_l = water density (kg/m^3)
ρ_s = solid density (kg/m^3)
ϕ_s = volume fraction of solids in slurry
d_p^j = particle diameter (m)

As the righthand side of Eq. 7 is a function of U_{sl}^j, the slip velocity is obtained by solving Eqs. 6 and 7 simultaneously.

The axial dispersion coefficient is calculated by a modification of the Finch and Dobby (1990) expression:

$$D = 0.063(1-\epsilon_g)\, d_c\left(\frac{J_g}{1.6}\right)^{0.3} \tag{8}$$

where
d_c = column diameter (m)
J_g = superficial air velocity (cm/s)

Equations analogous to Eqs. 1–8 are valid for the gangue particles, but with a considerably lesser effective flotation rate constant $k_g(d_p^j)$.

In the limit as $\Delta z \to 0$ the above difference equations become

$$\frac{\partial C_p^j}{\partial t} = \left(\frac{U_p}{1-\epsilon_g} - U_{sl}^j\right)\frac{\partial C_p^j}{\partial z} + D\frac{\partial^2 C_p^j}{\partial z^2} - k_p\left(d_p^j\right)C_p^j \tag{9}$$

for the section above the feed and

$$\frac{\partial C_p^j}{\partial t} = \left(\frac{U_t}{1-\epsilon_g} + U_{sl}^j\right)\frac{\partial C_p^j}{\partial z} + D\frac{\partial^2 C_p^j}{\partial z^2} - k_p\left(d_p^j\right)C_p^j \tag{10}$$

for the section below the feed.

Recovery (%) is defined as the ratio of the weight of the phosphate in the concentrate stream to the weight of the phosphate in the feed. The recovery for phosphate particles of the jth mesh size can be expressed in terms of the feed and tailings flow rates and concentrations as

$$R_p^j = \left(\frac{Q_f C_f^j - \left[Q_t + A_c(1-\epsilon_g)U_{sl}^j\right]C_{p_n}^j}{Q_f C_f^j}\right) * 100 \tag{11}$$

Grade, a measure of the quality of the product, is defined as the ratio of the weight of the phosphate to the total weight recovered in the concentrate stream. Grade is usually reported as % Bone Phosphate of Lime (%BPL), which is the equivalent grams of tricalcium phosphate, $Ca_3(PO_4)_2$, in 100 g of sample. For the typical Florida rock, mineral that contains no gangue is 73.3 % BPL. Grade can be obtained as the ratio of phosphate to the sum of phosphate and gangue in the product:

$$G^j = \left(\frac{Q_f C_f^j - \left[Q_t + A_c(1-\epsilon_g)U_{sl}^j\right]C_{p_n}^j}{\left(Q_f C_f^j - \left[Q_t + A_c(1-\epsilon_g)U_{sl}^j\right]C_{p_n}^j\right) + \left(Q_f C_{f_g}^j - \left[Q_t + A_c(1-\epsilon_g)U_{sl}^j\right]C_{g_n}^j\right)}\right) * 73 - 3 \tag{12}$$

where $C_{g_n}^j$ is gangue concentration of jth particle size in the nth layer and $C_{f_g}^j$ is the gangue feed concentration of jth particle size.

Calculation of Model Parameters

Since air holdup ϵ_g is measured experimentally, the above FPM has only two unmeasured model parameters for each particle size, namely, the flotation rate constants for phosphate (k_p) and for gangue (k_g). The experimental analysis usually available in industrial flotation columns is in terms of grade and recovery of phosphate. Let W_{fp}^j denote the weight of jth size phosphate particles in the feed, W_{fg}^j the weight of jth size gangue in the feed, and W_g^j the weight of jth size gangue in the product. The grade of feed is then

$$G_f^j = 73.3\frac{W_{fp}^j}{W_{fp}^j + W_{fg}^j} \tag{13}$$

and G^j is given by an analogous expression. The recovery of gangue can be readily calculated from measurements of grade and recovery of phosphate using the following relationship:

$$R_g^j = \frac{W_g^j}{W_{fg}^j} = \frac{R_p^j G_f^j(73.3 - G^j)}{G^j\left(73.3 - G_f^j\right)} \tag{14}$$

In some cases, direct measurements of the majority of gangue as acid insolubles may be available. Then more reliable estimates of R_g^j can be obtained by averaging values calculated from measurements of acid insolubles with values calculated from Eq. 14. This was done in this work.

From the FPM equations follows that the recovery of phosphate depends only on k_p, while the recovery of gangue depends only on k_g. This can be exploited to easily invert the steady-state version of the model to determine from experimental measurements of R_p^j and G^j corresponding to k_p and

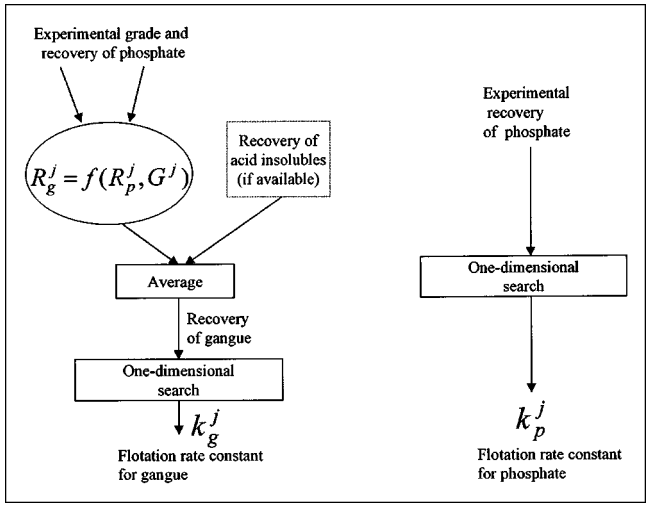

Figure 2. Flotation rate constants for phosphate and gangue calculated by 1-D search to invert the first-principles model.

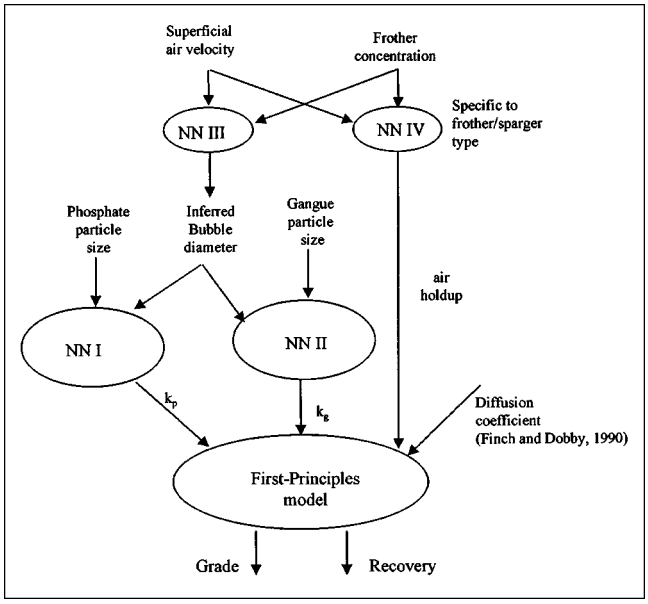

Figure 3. Overall structure of the hybrid model.

k_g. As shown in Figure 2, this is accomplished with one-dimensional searches. The search for k_p is initialized with two values that yield errors in the corresponding recovery R_p^j of opposite sign. Since typically $0 \le k_p \le 10\ \text{min}^{-1}$, the values of 0 and 100 min^{-1} are used. Then, the method of false position (Chapra and Canale, 1988) is used to iterate until the magnitude of the error in R_p^j drops to less than 10^{-3}. It is possible that the calculated recovery has a higher value than the experimental even for $k_p = 0$. In these cases, k_p is set equal to zero. The above procedure is also used to determine k_g, except that the high initial value is set to 10 min^{-1}.

Hybrid Model

The main factors affecting the air holdup ϵ_g are the superficial air velocity J_g and the frother concentration C_{frother}. Several factors affect the flotation rate constants, k_p and k_g, including particle diameter, superficial air velocity, frother concentration, collector concentration, extender concentration, and pH. In this study, we conducted experiments varying particle size, frother type, frother concentration, and superficial air velocity, and develop a hybrid model that portrays the effect of these factors on the performance of the column. The hybrid model utilizes backpropagation ANNs (Rumelhart et al., 1986) to predict the values of the parameters ϵ_g, k_p and k_g.

The straightforward approach is to develop an ANN for each of the three parameters. The inputs of the ANNs that predict k_p and k_g would be d_p, J_g, and C_{frother}, while the inputs of the ANN that predicts ϵ_g would be J_g, and C_{frother}. Each of the ANNs in this structure would then depend on the frother and sparger used. A change in the type of frother would mean that the previously trained ANNs are no longer applicable and would necessitate collection of a new set of training data and retraining of the networks. As changes in frother or sparger are not uncommon, this is a disadvantage.

The main reason J_g and C_{frother}, as well as the type of frother and sparger, affect the flotation rate constants is because they significantly affect the bubble size. An alternative hybrid model architecture is shown in Figure 3. The neural networks are structured in two levels. The first level consists of the ANNs for predicting k_p (NNI) and k_g (NNII), and receives as an input the inferred bubble size. This is the output of one of the ANNs of the second (top) level, NNIII. The second level also includes NNIV, which predicts air holdup. The advantage of this structure is that NNI and NNII are independent of the type of frother and sparger used, and therefore would not need retraining if they change.

As bubble size is not measured in industry, we infer it from the two-phase (air/water) air holdup, J_g, and U_t using the well-known Drift-flux analysis (Yianatos, 1988). The output required to train NNIV is the (two-phase) air holdup. Since air holdup is relatively easy to obtain, after a change of frother or sparger the hybrid model of Figure 3 can become functional in a short interval of time.

Materials and Methods

Experimental setup and procedures

Two types of experiments were conducted: two-phase (air/water) experiments to train neural networks NNIII and NNIV, and three-phase experiments to train NNI and NNII and to test the performance of the hybrid model.

The experimental setup for the three-phase experiments is shown in Figure 4. It included an agitated tank (conditioner) for reagentizing the feed, a screw feeder for controlling the rate of reagentized feed, and a flotation column. The 45-cm-diameter, 75-cm-high agitated tank is equipped with an impeller with two axial blades (each 28 cm diameter). The impeller had about 3.8 cm clearance from the bottom of the tank, and its rotation speed was fixed at 465 rpm. The feeder with a 2.5-cm-diameter screw delivered the conditioned phosphate materials to the column. The feed rate was controlled by adjusting the screw rotation speed. The 14.5-cm-diameter, 1.82-m-high flotation column was constructed of plexiglass.

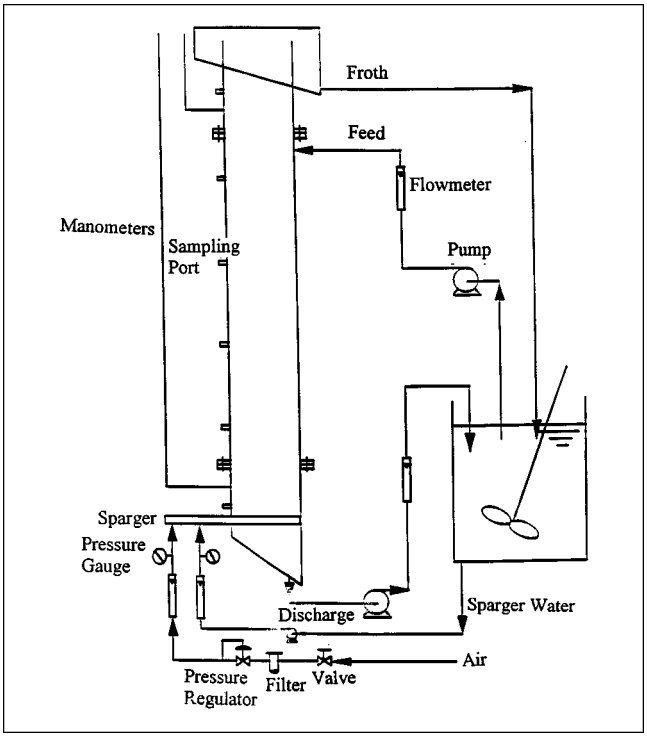

Figure 4. Experimental setup.

The feeding point was located at 30 cm from the column top. The discharge flow rate was controlled by a discharge valve and an adjustable speed pump. Three flowmeters were used to monitor the flow rates for air, frother solution, and elutriation water.

Phosphate feed (14×150 Tyler mesh) from Cargill was used as the feed material. For each run, 50 kg of feed was introduced to the pretreatment tank and water was added to obtain 72% solids concentration by weight. The tank was then agitated for 10 s. Solution of 10% soda ash was added to the pulp to reach pH of about 9.4, and the slurry was agitated for another 10 s. Subsequently, a mixture of fatty acids (a mixture of oleic, palmetic, and linoleic acid obtained from Westvaco) and fuel oil (No. 5 obtained from PCS Phosphates) with a ratio of 1:1 by weight was added to the pulp and the slurry continued to be mixed. The total conditioning time was 3 min. The conditioned feed material (without its conditioning water) was subsequently loaded to the feeder bin located at the top of the column.

Four frothers were used, two commonly employed in industry, F-507 (a mixed polyglycol by Oreprep) and CP-100 (a sodium alkyl ether sulfate by Westvaco), and two experimental, F-579 (also a mixed polyglycol by Oreprep) and OB-535 (by O'Brien). Frother-containing water and air were first introduced into the column through the sparger (an eductor) at a fixed water flow rate and frother concentration ($0-30$ ppm), and the superficial air velocity ranged from $0.24-0.94$ cm/s. Then, the discharge valve and pump were adjusted to get the desired underflow and overflow rates. Air holdup was measured using a differential pressure gauge. After the water/air system reached steady state, the screw feeder was started. To achieve steady feed rate to the column, water was added to the screw feeder at the rate that reduced the solids concentration to approximately 66% by weight. The column was run for a period of 3 min with phosphate feed prior to sampling. Timed samples of tailings and concentrates were taken. The collected product samples, as well as feed samples, were dried, sieved using Tyler meshes, weighed and analyzed for %BPL following the procedure recommended by the Association of Florida Phosphate Chemists (AFPC Analytical Methods, 1980). In addition, gangue content (as % acid insolubles) of the feed, tailings, and concentrate streams was measured (AFPC Analytical Methods, 1980). These measurements were then used to calculate recovery of acid insolubles. Subsequently, these values were averaged with the values obtained from Eq. 14 to obtain the R_g^j used to determine the flotation rate constants for gangue.

The two-phase experiments were identical to the three-phase experiments, except that no solid feed was introduced to the column, and the experiments were terminated when the water/air system reached steady state.

Neural network structure and training

NNI, NNII, NNIII, and NNIV of Figure 3 were feedforward backpropagation artificial neural networks with a single layer of hidden nodes between the input and output layers and a unit bias connected to both the hidden and output layers. Inputs and outputs were scaled from 0 to 1. The hidden and output layer nodes employed logistic activation functions (Hertz et al., 1992).

For each of the four frothers investigated, 28 two-phase experiments were conducted (full factorial design with seven frother concentrations and four superficial air velocities). These were used to train (19 data points) and to validate (9 data points) the top level neural networks (NNIII and NNIV), a different pair for each frother. Three-phase runs yielded 28 experimental grades and recoveries, which were used to train (19 data points) and to validate (9 data points) NNI and NNII. To set the number of nodes in the hidden layer of each network, the number was increased until the sum of the absolute errors of the training and validation outputs started increasing. In this manner, an appropriate number of hidden nodes was determined to be three for all the neural networks.

The training process started by initializing all weights randomly to small nonzero values. The random numbers were generated in the range -3.4 to $+3.4$ with a standard deviation of 1.0 following the procedure recommended by Masters (1993). The optimal weights were determined by combining simulated annealing (Kirkpatrick et al., 1983) with the Polak-Ribiere conjugate gradient algorithm (Polak, 1971). Simulated annealing randomly perturbed the independent variables (the weights) and kept track of the best (lowest error) function value for each randomized set of variables. This was repeated several times, each time decreasing the variance of the perturbations with the previous optimum as the mean. Then, the conjugate gradient algorithm was used to minimize the mean-squared output error. When the minimum was found, simulated annealing was used to attempt to break out of what may be a local minimum. This alternation was continued until a lower point could not be found. This approach improves the likelihood of convergence to the global optimum.

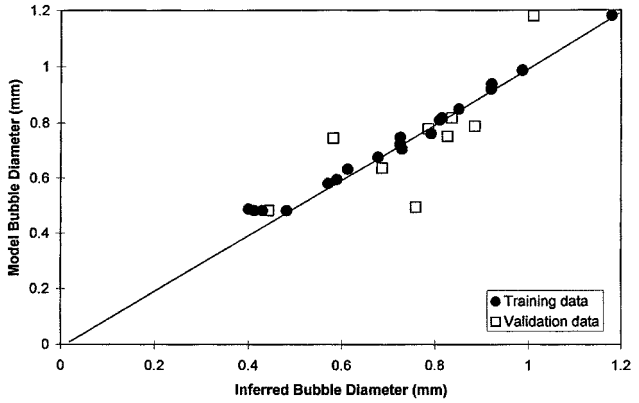

Figure 5. Performance of NNIII: model bubble diameter vs. bubble diameter from experimental data when CP-100 was the frother.

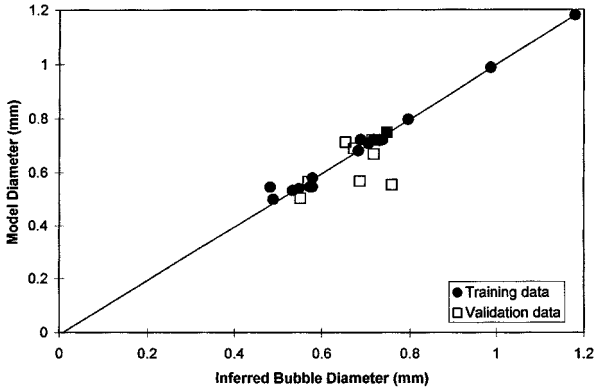

Figure 6. Performance of NNIII: model bubble diameter vs. bubble diameter from experimental data when F-507 was the frother.

Results and Discussion

The performance of the network for predicting bubble diameter (NNIII), the network for predicting air holdup (NNIV), a network for predicting the phosphate flotation rate constant (NNI) and the network for predicting the gangue flotation rate constant (NNII) is shown in Figures 5–16. Figure 5 compares the NNIII output to the inferred bubble diameter using experimental data when the frother was CP-100. The solid circles are for the data used for training while the open squares are for the data used for validation. Figures 6, 7 and 8 shows the performance of NNIII when F-507, OB-535, and F-579, respectively, were the frothers. As these figures show, NNIII successfully predicts the inferred bubble diameter. Figure 9 compares the air holdup predicted by NNIV to the experimental values measured by a differential pressure cell when CP-100 was used as the frother. Figures 10, 11 and 12 show the performance of NNIV when F-507, OB-535, and F-579, respectively, were used as frothers. As shown in these figures, NNIV successfully predicts the air holdup for all frothers.

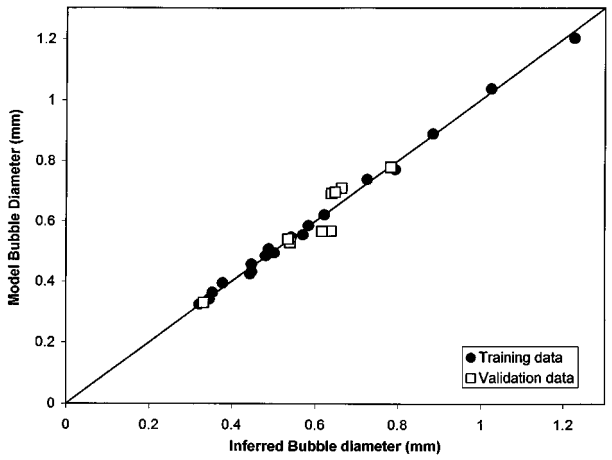

Figure 7. Performance of NNIII: model bubble diameter vs. bubble diameter from experimental data when OB-535 was the frother.

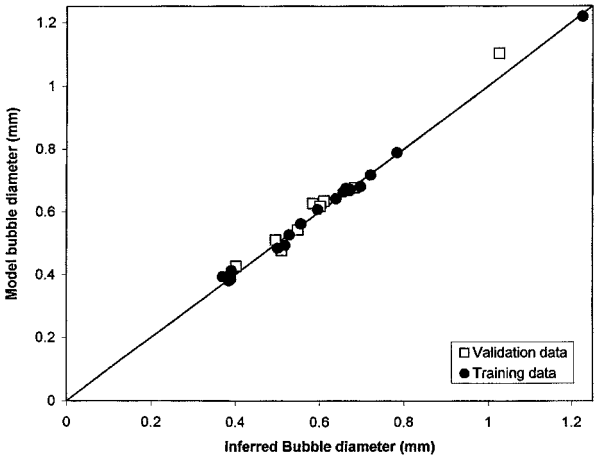

Figure 8. Performance of NNIII: model bubble diameter vs. bubble diameter from experimental data when F-579 was the frother.

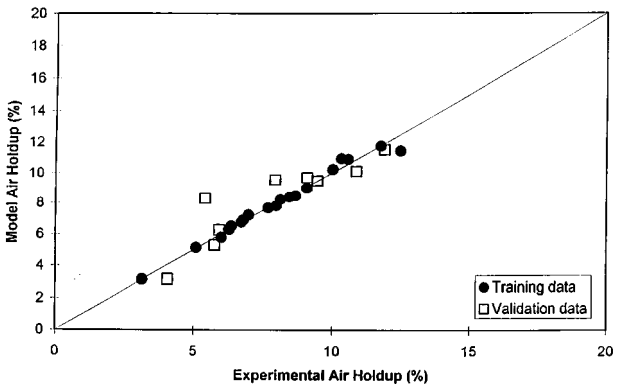

Figure 9. Performance of NNIV: model vs. experimental air holdup for frother CP-100.

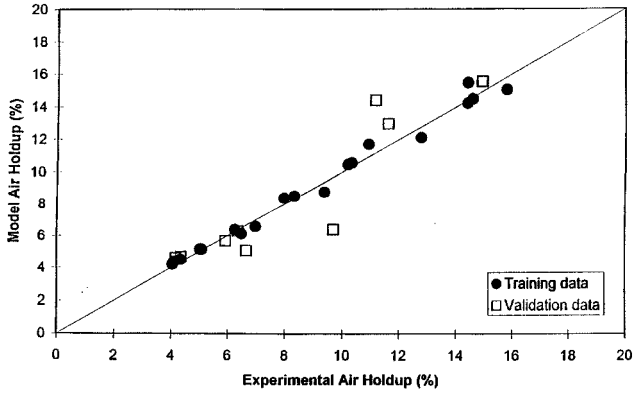

Figure 10. Performance of NNIV: model vs. experimental air holdup for frother F-507.

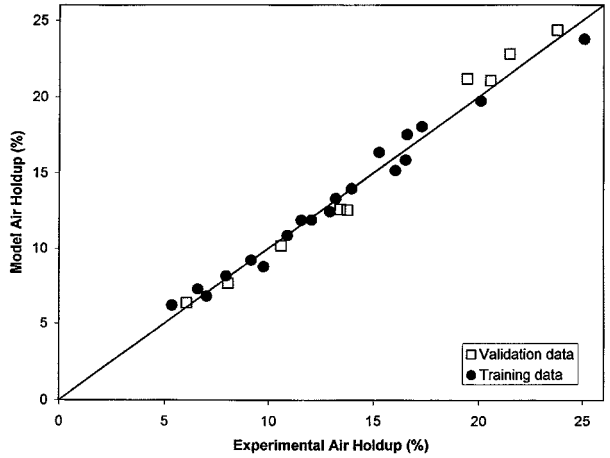

Figure 11. Performance of NNIV: model vs. experimental air holdup for frother OB-535.

Figures 13 and 14 show the performance of NNI and NNII, respectively. Figure 13 presents the predicted flotation rate constants for phosphate (k_p) against those determined from

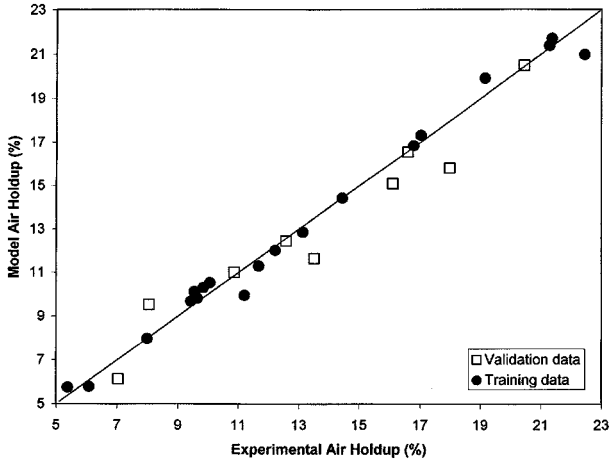

Figure 12. Performance of NNIV: model vs. experimental air holdup for frother F-579.

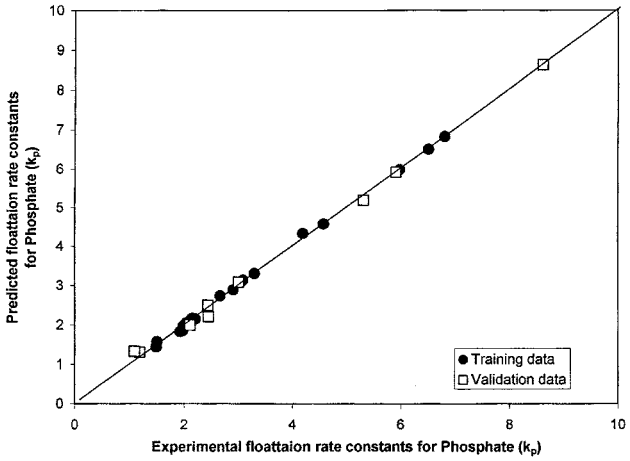

Figure 13. Performance of NNI: model vs. experimental flotation rate constant for phosphate (k_p).

one-dimensional searches using experimental data. As shown in this figure, NNI does accurately predict low and high values of flotation rate constants. Figure 14 presents the flotation rate constants for gangue (k_g) predicted using NNII against those determined from experimental data. A very good match is seen.

The hybrid model integrates NNI, NNII, NNIII, and NNIV with the FPM as shown in Figure 3. Predictions of the hybrid model are shown in Figures 15 and 16. Figure 15 presents the predicted recovery (%) against the experimental recovery for frother CP-100 (square points), F-507 (circles), OB-535 (triangles), and F-579 (diamonds). Similarly, Figure 16 compares the predicted grade (%BPL) against the experimental grade for CP-100, F-507, OB-535, and F-579. It can be seen from these figures that predicted recovery and grade from the hybrid model match closely the experimental values, with the exception of one grade for OB-535. The root mean squared errors in predicted recovery were 0.1%, 0.2%, 1.5%, and 0.4% for CP-100, F-507, OB-535, and F-579, respectively. The root mean squared errors in predicted grade were 3.2 %BPL, 1.5

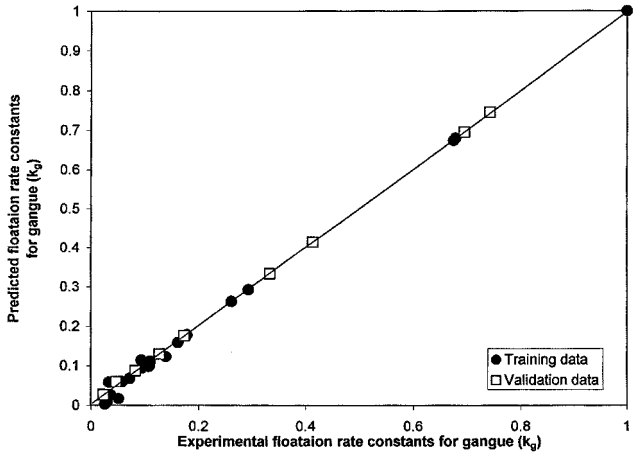

Figure 14. Performance of NNII: model vs. experimental flotation rate constant for gangue (k_g).

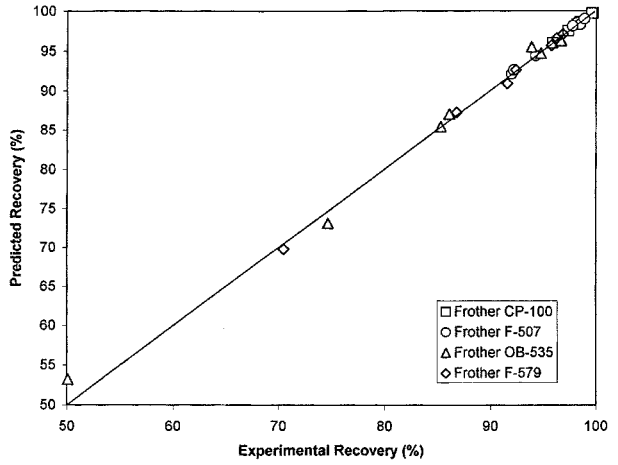

Figure 15. Performance of the overall hybrid model: predicted vs. experimental recovery (%) for the four frothers.

%BPL, 7.5 %BPL, and 1.5%BPL for CP-100, F-507, OB-535, and F-579, respectively.

An alternative to this modeling approach is to develop a pure neural-networks model. This would, however, require a large number of inputs: not only superficial air velocity, frother concentration, and particle size, but also feed flow rate, feed concentration, elutriation flow rate, tailings flow rate, and solids loading. This increase in the number of inputs to eight would increase the number of weights (model parameters) needed and therefore the number of three-phase data required for training. Furthermore, as with an in-series hybrid model that uses one level of neural networks, a change in frother or sparger would require generating a new set of data and retraining all the networks. The hybrid model presented here with the two levels of neural networks involves a relatively low number of inputs in the artificial neural networks, does not require new three-phase data if a frother or sparger are changed, and predicts very well both grade and recovery excellently.

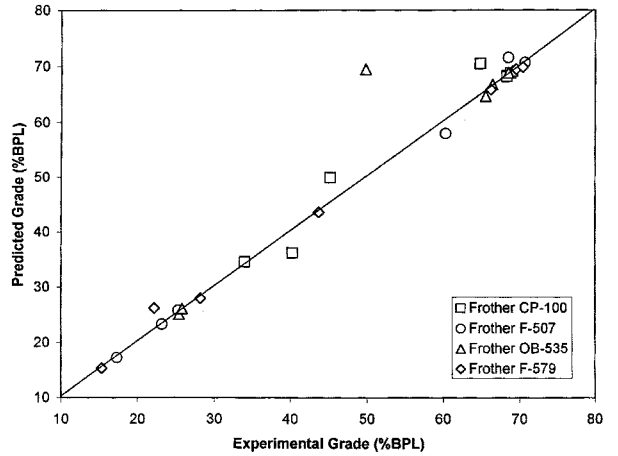

Figure 16. Performance of the overall hybrid model: predicted vs. experimental grade (%BPL) for the four frothers.

Conclusions

A hybrid neural network modeling approach was used to model a flotation column for phopshate/gangue separation. This model comprises two parts, a first-principles model, and two levels of neural networks that serve as parameter predictors of difficult-to-model process parameters. Experimental data from a laboratory column were used to train and validate the neural networks, and the hybrid model captures the dependence of column performance on particle size, frother concentration, and superficial air velocity.

Acknowledgments

The authors wish to thank Florida Institute of Phosphate Research, Bartow, FL, and the National Science Foundation (Grant #9312369 BES) for financial support for this project. Additional funding was provided by the Engineering Research Center for Particle Science and Technology at the University of Florida, the National Science Foundation grant #EEC-94-02989, and the Industrial Partners of the ERC.

Literature Cited

Assoc. of Florida Phosphate Chemists, *AFPC Analytical Methods*, 6th ed. (1980).

Chapra, S. C., and R. P. Canale, *Numerical Methods for Engineers*, McGraw Hill, New York (1988).

Cubillos, F. A., and E. L. Lima, "Identification and Optimizing Control of a Rougher Flotation Circuit using an Adaptable Hybrid-Neural Model," *Minerals Eng.*, 10, 707 (1997).

Cubillos, F., P. Alvarez, J. Pinto, and E. Lima, "Hybrid-Neural Modeling for Particulate Solid Drying Processes," *Powder Technol.*, **87**, 153 (1996).

Dobby, G. S., and J. A. Finch, "Column Flotation: A Selected Review: II," *Mineral Eng.*, **4**, 911 (1991).

Dobby, G. S., and J. A. Finch, "Mixing Characteristics of Industrial Flotation Columns," *Chem. Eng. Sci.*, **40**, 1061 (1985).

Finch, J. A., and G. S. Dobby, *Column Flotation*, Pergamon Press, Toronto (1990).

Hertz, J., A. Krogh, and R. G. Palmer, "Introduction to the Theory of Neural Computations," 5th ed., Addision-Wesley, Redwood City, CA (1992).

Hornik, K. M., M. Stinchcombe, and H. White, "Multi-layer Feedforward Networks are Universal Approximators," *Neural Networks*, **2** 359 (1989).

Johansen, T. A., and B. A. Foss, "Representing and Learning Unmodeled Dynamics with Neural Network Memories," *Proc. Amer. Control Conf.*, Vol. 3, p. 3037, Chicago (1992).

Kirkpatrick, S., Jr., C. D. Gelatt, and M. P. Vecchi, "Optimization by Simulated Annealing," *Science*, **220**, 671 (1983).

Kramer, M. A., and M. L. Thompson, "Embedding Theoretical Models in Neural Networks," *Proc. Amer. Control Conf.*, Vol. 1, p. 475, Chicago, (1992).

Liu, P.-H., T. Potter, S. A. Svoronos, and B. Koopman, "Hybrid Model of Nitrogen Dynamics in a Periodic Wastewater Treatment Process," AIChE Meeting, Paper No. 195 (1995).

Luttrell, G. H., and R. H. Yoon, "A Flotation Column Simulator Based on Hydrodynamic Principle," *Inter. J. Miner. Process*, **33**, 355 (1992).

Luttrell, G. H., and R. H. Yoon, "Column Flotation−A Review," *Beneficiation of Phosphate: Theory and Practice*, H. El-Shall, B. M. Moudgil and R. Wiegel, eds., SME, p. 361 (1993).

Masters, T., *Practical Neural Network Recipes in C++*, Academic Press, New York (1993).

Mavros, P., "Mixing in Flotation Columns: 1: Axial Dispersion Modeling," *Mineral Eng.*, **6**, 465 (1993).

Perry, R. H., D. W. Green, and J. O. Maloney, "Perry's Chemical Engineers Handbook," 6th ed. McGraw-Hill, New York (1984).

Polak, E., *Computational Methods in Optimization*, Academic Press, New York (1971).

Psichogios, D. C., and L. H. Ungar, ''Process Modeling using Structured Neural Networks,'' *Proc. Amer. Control. Conf.*, Vol. 3, p. 1917, Chicago (1992).
Psichogios, D. C., and L. H. Ungar, ''A Hybrid Neural-Network First Principles Approach to Process Modeling,'' *AIChE J.*, **38**, 1499 (1992).
Reuter, M., J. Van Deventer, and P. Van Der Walt, ''A Generalized Neural-Net Rate Equations,'' *Chem. Eng. Sci.*, **48**, 1281 (1993).
Rumelhart, D. and J. McClelland, *Parallel Distributed Processing*, MIT Presse, Cambridge, MA (1986).
Sastry, K. V. S., and K. D. Loftus, ''Mathematical Molding and Computer Simulation of Column Flotation,'' *Column Flotation*, K. V. S. Sastry, ed., SME-AIME, p. 57 (1988).
Su, H.-T., P. A. Bhat, P. A. Minderman, and T. J. McAvoy, ''Integrating Neural Networks with First Principles Models for Dynamic Modeling,'' *IFAC Symp. On Dynamics and Control of Chemical Reactors, Distillation Columns, and Batch Processes*, (1992).
Thompson, M. L., and M. A. Kramer, ''Modeling Chemical Processes Using Prior Knowledge and Neural Networks,'' *AIChE J.*, **40**, 1328 (1994).
Villeneuve, J., M.-V Durance, C. Guillaneau, A. N. Santana, R. V. G. da Silva, and M. A. S. Martin, ''Advanced Use of Column Flotation Models for Process Optimization,'' *Column*, C. O. Gomez, and J. A. Finch, eds., Metall. Soc. of the Can. Inst. of Mining, Metall. and Pet., p. 51 (1996).
Xu, M., and J. A. Finch, ''The Axial Dispersion Model in Flotation Column Studies,'' *Mineral Eng.*, **4**, 553 (1991).
Yeager, D., C. L. Karr, and D. A. Stanley, ''Column Flotation Model Tuning Using a Genetic Algorithm,'' SME Meeting, Preprint 95 (1995).
Yianatos, J. B., J. A. Finch, G. S. Dobby, and M. Xu, ''Bubble Size Estimation in a Bubble Swarm,'' *J. Colloid Interf. Sci.*, **126**, 37 (1988).
Yoon, R. H., G. H. Luttrell, and G. T. Adel, ''Advances in Fine Particle Flotation,'' *Challenges in Mineral Processing*, K. V. S. Sastry and M. C. Fuerstenau, eds., SME-AIME, p. 487 (1989).
Yoon, R. H., G. H. Luttrell, G. T. Adel, and M. J. Mankosa, ''Recent Advances in Fine Coal Flotation,'' *Advances in Coal and Mineral Processing Using Flotation*, S. Chandler and R. R. Klimpel, eds., SME-AIME, p. 211 (1988).

Manuscript received June 1, 1998, and revision received Jan. 20, 1999.